Knockout reactions: experimental aspects*

Dolorès Cortina Gil

Universidad de Santiago de Compostela,
E-15782 Santiago de Compostela, España

Résumé

La disponibilité des faisceaux instables a favorisé le développement d'une activité importante dans le domaine des réactions directes. Dans le cas particulier des faisceaux exotiques de haute énergie, les réactions de cassure des projectiles, appelées réactions de knockout dans ce texte, ont été très intensivement étudiées. Ce cours donne une vue d'ensemble des résultats expérimentaux obtenus en appliquant cette technique. La sensibilité de la méthode aux différents aspects expérimentaux est illustrée par la description de quelques cas particuliers. L'utilisation des réactions de knockout en tant qu'outil spectroscopique est discutée en détail.

Abstract

The availability of radioactive beams has given rise to intense activity in the field of direct reactions. The removal of one(two)-nucleon (referred to as nucleon knockout in this text) from a fast exotic projectile has been extensively investigated. This lecture provides a general overview of the experimental results achieved using this technique. The sensitivity of the method to different experimental aspects is illustrated with a few examples. Special attention is given to the application of nucleon-knockout reactions as a general purpose spectroscopic tool.

Contents

*This lecture is complementary to the one given by Daniel Baye(in this school) where theoretical aspects of dissociation reactions are introduced

1 Introduction

Let's consider a fast projectile approaching a target at rest. Once the projectile and the target are close enough, they will react. The nature of the projectile-target interaction can be nuclear (light target) or Coulomb (heavy target) in its origin. For large impact parameters, the reaction would be peripheral, and would result in the dissociation or breakup of the projectile into one (or a few) nucleon(s) (neutrons or protons) that would be ejected at large angles and a quasi-projectile (very often called core-fragment) that would continue its path almost unaffected by the reaction, with almost the same energy as the projectile.

At projectile relativistic energies, these reactions are considered to be direct. They proceed in a single step and the reaction mechanism can be formally described using semi-classical approximations (see details in D. Baye lecture). Comparatively, this "simple" reaction channel, associated with the removal of a single (few) nucleon, is quite favoured, giving these processes relatively high cross-sections.

These reactions have been used to elucidate the wave function of exotic nuclei (projectile). The superposition of different removed-nucleon + core-fragment configurations resulting after breakup creates a realistic picture of the original exotic projectile wave function. Therefore, the projectile wave function can be factorised as:

$$|Projectile>=\sum C^2S(|core>\otimes|nucleon>) \quad (1)$$

where $|core>$ and $|nucleon>$ represent the core-fragment and removed nucleon wave function and C^2S are the spectroscopic factors associated with each configuration.

The aim of this lecture is to provide an overview of the achievements and limitations related to the application of knockout reactions as spectroscopic tools, with special emphasis on the experimental aspects of the method. The lecture is structured around the presentation of a few selected experimental examples. Some of them, where the determination of the physical observables depends entirely on the detection of the emerging core-fragment after knockout, are known as inclusive measurements. These measurements would provide a weighted picture of the different core-fragment + removed-nucleon that form the structure of the ground state of the exotic projectile under study. In other cases, the core-fragment detection will be complemented by its eventual gamma de-excitation. These are known as exclusive measurements, and are sensitive to the individual core-fragment + removed nucleon contributions of the ground

state of the exotic projectile. They would provide experimental access to the corresponding spectroscopic factors.

Different names have been used in the literature to refer to these kind of reactions (i.e.: nucleon removal, nucleon breakup and nucleon knockout). This last name was adopted by the NSCL community in their publications and is probably the most widely used (see review articles and references therein [1, 2, 3]). The choice of this name was not naive, it was already used more than three decades ago to refer to quasi-free scattering reactions induced either by high energy protons and electrons, (p,2p) and (e,e'p), known to be very powerful spectroscopic tools. Indeed "proton-knockout" using high-energy electrons (e,e'p) was studied extensively in the 1980s, and was considered the only experimental method able to provide absolute spectroscopic factors in well-bound nuclei [4, 5].

Here we will use the term "knockout reactions" to refer to these reaction channels. Figure 1 shows the reaction mechanism for the particular case of two-proton knockout of a ^{28}Mg projectile by a light ^{9}Be target (discussed later in section 7).

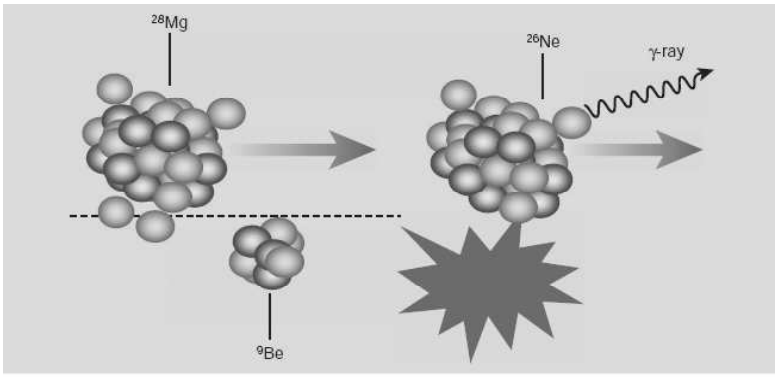

Figure 1: *Schematic representation of a two-proton knockout of an unstable ^{28}Mg projectile at $\approx$ 67 MeV/nucleon by a stable beryllium target [6, 7]. Two of the four loosely bound protons are removed during the reaction, leaving a core of ^{26}Ne.*

,

Most of this lecture is dedicated to the particular case of one-nucleon nuclear knockout reactions, induced by light targets. The particular cases of one-nucleon Coulomb (interaction with heavy targets) knockout and two-nucleon knockout reactions will be discussed in the last sections. Interested readers can find complementary information in the following review articles [1, 2, 3], and their references.

2 Reactions with fast radioactive beams

The interest in exploring the structure of nuclei far from the β stability valley is not a recent topic in modern nuclear physics. The first experiments with radioactive secondary beams were performed more than fifty years ago ([8] and references therein). They were limited to the available experimental tools and concentrated on radioactivity experiments (i.e.: decay radiation, masses and determination of ground-state properties). Subsequent technological progress made it possible to apply techniques that had been developed for stable beams to the case of secondary beams. An example of this is the intense transfer reactions program developed with

secondary beams at GANIL in the last few years [9].

The advent of fast radioactive beams produced by projectile fragmentation and the development of the in-flight identification technique for the emerging fragments was an important milestone in the systematic study of unstable nuclei. It is important to mention the pioneering work of Tanihata and collaborators in the systematic investigations of matter radii of exotic nuclei [10, 11]. A few years latter, nucleon-knockout [13] was used for the first time to obtain spectroscopic information on unstable nuclei. Since then, this method has been used extensively.

Nucleon-knockout and transfer reactions are quite complementary. Both methods are considered excellent spectroscopic tools and allow the microscopic structure of a given nucleus to be determined in its ground and excited states. Transfer reactions yield high cross sections (1mb) at relatively low energies (in the range 20-30 MeV/nucleon) whereas the optimum range for knockout reactions is associated with projectile energies around 100 MeV/nucleon and higher. The cross section of this process can vary from well above 100 mb, for loosely bound nuclei, to 1 mb for tight nuclei. In a good approximation, at beam energies above 60-70 MeV/nucleon, the internal degrees of freedom in a nucleus can be considered "frozen" during the collision [12]. Within this picture known as "adiabatic approximation" the momentum of the recoil fragment after one-nucleon removal provides a measurement of the wave function of the removed nucleon. Another big advantage of working at higher energies is that the reaction mechanism description is simplified, which permits the use of a semi-classical approximation of the reaction with regard to the impact parameter of the relative motion of projectile and target.

The knockout process to a given final state includes different contributions. "Stripping" or inelastic breakup refers to cases where the removed nucleon reacts with the target, the nucleon is scattered to large angles and the target is excited. "Diffraction" or elastic breakup, corresponds to reactions where the target remains in its ground state and the removed nucleon is emitted in forward direction, almost at the projectile velocity. The third contribution, called Coulomb dissociation, corresponds to electromagnetic elastic breakup and plays a minor role in the case of light targets (see details in D. Baye's lecture and [1]). The so-called single particle cross-section (σ_{sp}) of the process can be expressed as:

$$\sigma_{sp} = \sigma_{str} + \sigma_{dif} + \sigma_{Cou} \tag{2}$$

where σ_{str}, σ_{dif} and σ_{Cou} stand for stripping, diffraction and Coulomb contributions, respectively .
In the most cases, the largest contribution is stripping , but for very loosely-bound nuclei (haloes) the role of "diffraction" can be important. Both contributions are very often calculated using "eikonal" or "Glauber" theory based in the assumption that the projectile's constituents follow straight-line paths- with constant velocity (see D. Baye's lecture and [1, 14]).

Different approaches have been used to compute these contributions. Originally they were calculated using the so-called "black disk" model, based on geometrical considerations. In this model, the stripping contribution leaves the wave function unchanged throughout space, except for a cylinder where it vanishes [15, 16, 17]. The idea behind it is the fact that all reactions with an impact parameter smaller than the sum of the target and core nucleus radii will destroy this last one. Consequently, this region of the wave function is never sampled in these reactions. The radius of the cylinder is chosen according to the effective target radius and the impact parameter, in order to reproduce empirical nucleon and core-target reaction

cross sections at the energies of interest. A more accurate picture of these single-particle cross sections is provided by the "spectator-core" approximation to the many-body eikonal theory. This approximation uses more realistic nucleon- and core-target elastic S-matrices than the black disk approximation. The expressions for stripping and diffractive single-particle cross sections are given by:

$$\sigma_{str} = \frac{1}{2j+1} \int d\vec{b} \sum_{m} < \Psi_{jm})|1 - |S_n|^2)|S_c|^2|\Psi_{jm} > \tag{3}$$

$$\sigma_{dif} = \frac{1}{2j+1} \sum_{\sigma,m} \int d\vec{k} \int d\vec{b} < \Psi_{\vec{k}\sigma}|1 - (S_n S_c)|\Psi_{jm} > |^2 \tag{4}$$

where Ψ_{jm} is the removed-nucleon core wave function and $|S_n|$ and $|S_c|$ are the S- matrices or projectile functions for the removed-nucleon target and core target. $\Psi_{\vec{k}}$ represent continuum breakup states. A detailed explanation of how these expressions are determined is presented by J. Tostevin in [59, 20, 18]. There are other approaches that do not involve these "adiabatic and eikonal" approximations such as [19, 21].

The cross section is then assumed to be the sum of all possible states of the product of the single-particle cross section (given by the sum in equation 2) and a spectroscopic factor (C^2S).

$$\sigma = \sum_{j} C^2S(nlj)\sigma_{sp}(S_n, nlj) \tag{5}$$

The spectroscopic factors reflect the "different probability of existence" associated to each particular configuration (see the N. Keeley and A. Poves lectures for details on the spectroscopic factor concept).
Cross sections determined in this way are compared with the experimentally obtained cross sections to deduce experimental spectroscopic information.

Another source of information comes from the momentum distribution of the remaining core-fragment. In the "sudden" approximation, the momentum distribution of the A-1 fragment in the rest frame of the projectile is equal (but with opposite sign) to the momentum of the removed nucleon. This core fragment momentum distribution provides information on the knockout nucleon wave function. The comparison of experimental core-fragment momentum distributions with theoretically evaluated distributions, taking into account removed nucleons in different orbits (with different angular momenta), would allow us to assign the angular momentum of the removed nucleon and subsequently the spin and parity of the ground state of the exotic nuclei being studied.

2.1 Experimental aspects

To perform a knockout experiment induced by exotic nuclei you need:

a) high-energy secondary beams

b) a detection system able to select the reaction channel and ensure a kinematically complete measurement (i.e: identification and tracking of projectiles and core-fragments, high precision measurement of the core-fragment moment and discrimination of the different possible core-fragment excites states).

Currently, high-energy secondary beams are produced by projectile fragmentation of stable beams that are generated by heavy ion accelerators such as synchrotrons and cyclotrons. Projectile fragmentation results in a cocktail beam composed of the various fragments that are produced. The final intensity of the secondary beams must be sufficient to guarantee the success of the experiment: a minimum intensity of a few particles per second is necessary to perform inclusive exploratory investigations. This intensity will depend on different factors. Among the most important are:

- the type of accelerator used: cyclotrons generally provide higher intensities than synchrotrons.
- the choice of projectile: the closer the primary projectile and the secondary beams are in A and Z, the higher the production cross section.
- the target thickness. Working at high energies makes it possible to use relatively thick targets, which have a larger number of atoms and thus a greater secondary particle yield.

Knockout experiments are performed using very powerful magnetic spectrometers. These devices are composed of a set of electric and magnetic elements that guarantee optimum transport of secondary projectiles and emerging fragments. Electromagnetic spectrometers also act as filters allowing the selection of one (or a few) secondary fragments from among all the species produced after fragmentation of the projectile. They are equipped with various detectors to ensure identification and tracking of ions traversing the system in an event-by-event basis. Last but not least, spectrometers provide a very accurate determination of the momentum of the nuclei, which makes it possible to translate the position distribution of the core fragments into the momentum change induced in a knockout target. Interested readers will find further details on those topics in P. Roussel-Chomaz's lectures (in this school) and [26].

Projectile fragmentation uses inverse kinematics, which means that the fast projectile is heavier than the target. This has interesting kinematic consequences. All fragments produced are emitted in forward direction at velocities similar to that of the projectile and with a relatively small angular aperture, which helps to increase the transmission of fragments through the spectrometer.

The energy of the secondary beam also plays an important role in determining experimental constraints. The higher the secondary beam energy, the smaller the angular aperture of the cone in which the reaction fragments are emitted. The result is a more efficient transmission of projectile and core-fragments through the magnetic spectrometer for higher energies.

3 Experimental determination of observables measured in knockout reactions

In this section we will introduce the observables needed to obtain experimental access to the exotic projectile wave function, namely the momentum distribution of the core-fragments resulting after nucleon knockout and the cross section associated with this reaction channel. The longitudinal momentum distribution of the core-fragment after knockout provides information about the wave function of the removed nucleon whereas spectroscopic factors (C^2S) are determined from the removal cross sections. Gamma de-excitation of the core-fragment can also be

measured with gamma detector arrays. The coincident detection of core-fragment momentum distribution and removal cross-section with gamma-rays provides information on each individual contribution to the exotic projectile wave function (see equation 1).

Figure 2 shows a schematic view of the generic experimental setup at the FRragment Separator (FRS) at GSI [23]. The determination of all the observables introduced in this section will be referred to this example. Other devices extensively used to perform measurements of this kind are the A1900/S800 spectrograph at NSCL/MSU [25] and the SPEG energy loss spectrometer at GANIL [24].

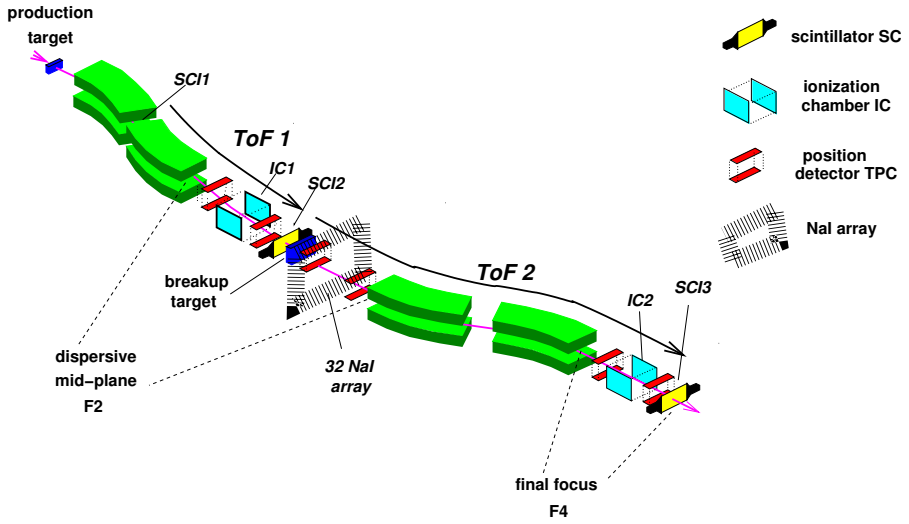

Figure 2: *A schematic view of the FRagment Separator (FRS) with its detection set-up. Complete identification with ToF (SC) and energy-deposition (IC) measurements is possible in both sections of the spectrometer. Several position sensitive detectors (TPC) provide projectile and fragment tracking as well as measurement of fragment momentum distribution. A γ detector (NaI) provides coincident measurement of fragments with its γ-ray deexcitation .*

The first section of the spectrometer is tuned to transport the nucleus of interest until it reaches to the intermediate image plane, where the knockout reaction is induced. Other fragmentation products that fit inside the spectrometer acceptance will be transported as well (as shown in the left panel of Figure 3). The spectrometer section behind the knockout target is then set to the magnetic rigidity of the ${}^{A-1}{}_{Z}\mathrm{X}$ fragments produced in the one-neutron knockout reaction (right panel of Figure 3).

At the same time, we also have to ensure an unambiguous selection of the reaction channel. This is achieved by the double identification of the exotic projectile before the knockout target and the remaining core-fragment after knockout target. Figure 3 illustrates a particular case corresponding to the ^{40}Ar fragmentation at 1 GeV/nucleon performed at the FRS. The first section of the spectrometer was tuned to select ^{20}O fragments (right panel), whereas the second section was tuned to select ^{19}O fragments emerging from the one-neutron knockout on a carbon target. In this particular measurement, identification was achieved by determining the A/Z ratio from Time of Flight (ToF) measurements with plastic scintillators, and energy losses ($\approx \mathrm{Z}^2$) recorded by ionisation chambers.

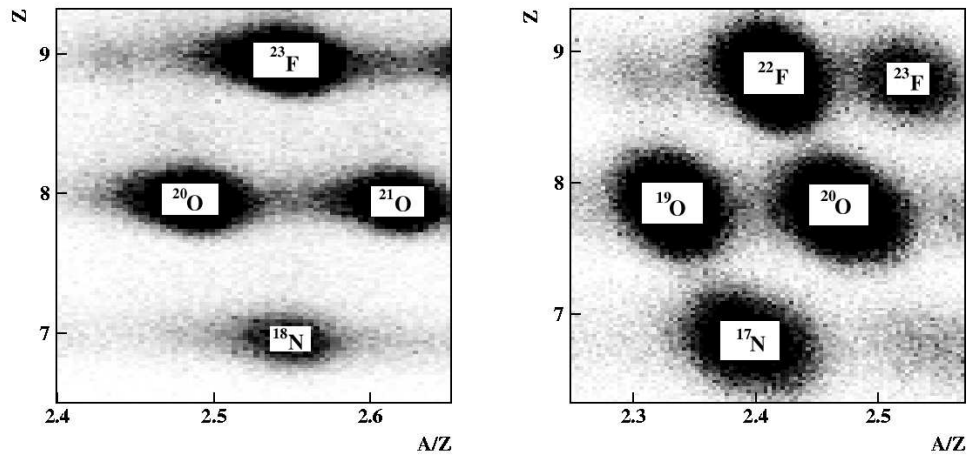

Figure 3: *Identification of different secondary beams (left) and the corresponding one-neutron removal core-fragments (right) emerging after one-neutron knockout on a carbon target. This cocktail beam was obtained by fragmentation of* ^{40}*Ar at 1 GeV/nucleon impinging on a Be target [22].*

In the "adiabatic" approximation mentioned in section 2, the momentum of the core-fragment after one-nucleon removal provides information on the wave function of the removed nucleon. Narrow momentum distributions have been associated with large spatial extension of the removed nucleon. This was clearly observed in experiments with halo nuclei that will be presented in detailed later in this lecture (section 5). In more general terms, core-fragment momentum distribution is sensitive to the angular momentum of the removed nucleon. For example, the momentum width due to knockout is around 50 MeV/c for an s (l=0) neutron, and around 300 MeV/c for a d (l=2) neutron. The core-fragment momentum is determined by measuring the velocity shift induced by the knockout target. To determine velocity shift, position sensitive detectors measure the position distribution of the one-nucleon removal residue at the final spectrometer focal plane.
It is important to keep in mind that the experimental determination of core-fragment momentum distributions requires high-resolution measurements, which are obtained by the use of spectrometers. The most stringent cases would correspond to the narrow momentum distributions of halo nuclei (see section 5), where a single-particle hole yields a FWHM in the order of 50-80 MeV/c in the core-fragment momentum distribution.

The momentum distribution of the core-fragment measured(p_f) at the final focus reflects the momentum shift induced in the knockout reaction. This momentum distribution is obtained from the positions of the fragments, measured at the reaction point(X_R) and final focus(X_F) according to the equation.

$$p_f = Q_f B\rho(1 + \frac{X_F}{D_2} + \frac{X_R}{D_1}) \tag{6}$$

where Bρ is the magnetic rigidity and D_1 and D_2 the dispersion of the different sections of

the spectrometer.
In theory, position distribution measurements are possible in the longitudinal and transversal directions to the beam direction. These quantities make it possible to determine the longitudinal (parallel) and transverse (perpendicular) contributions with respect to the beam direction of the core-fragment momentum distribution. Both projections should contain the same information but the longitudinal distribution is preferred because it is less affected by Coulomb diffraction and diffractive scattering mechanisms (see section 2 and references therein).

From now on, we will always refer to core-fragments longitudinal momentum distributions. The experimental determination of the core-fragment momentum distribution is measured in the laboratory reference system and then transformed to the co-moving system using the corresponding Lorentz transformation.

The final core-fragment momentum resolution depends not only on the tracking and magnetic solving power but also on the quality of the primary beam (spot size and angular alignment) and the amount of matter at the mid-plane (angular energy straggling). Most of these contributions can be experimentally evaluated by measuring the momentum distribution of the projectile (without knockout target)[28, 27], which can be used for deconvolution (FWHM reported in literature are always corrected by this value). Figure 4 shows these effects for the case of ^{19}C at 910 MeV/nucleon.

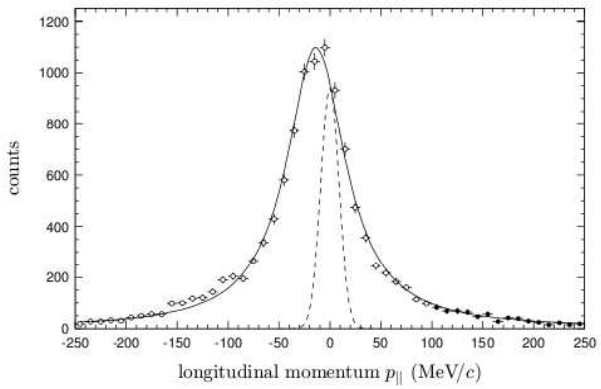

Figure 4: *Longitudinal momentum distribution of ^{18}C fragments from one-neutron knockout of ^{19}C at 910 MeV/nucleon on a carbon target. The dashed profile represents the measured system resolution with a width of 19.9 MeV/c [27].*

The left panel in Figure 5 shows core-fragments momentum distributions of different carbon projectiles, at almost 1 GeV/nucleon, after one-neutron knockout ranging from the bound case of ^{12}C with a FWHM of 220 ± 12 MeV/c to the loosely bound ^{19}C with a FWHM of 71 ± 3 MeV/c. These experimental results show the different nature of the removed neutron, and indicate the presence of an s-neutron in ground state configuration in the one-neutron halo nuclei ^{19}C [28].

The one-nucleon removal cross section is deduced from the ratio between the exotic projectile, which comes from direct counting of the number of projectiles in front of the knockout

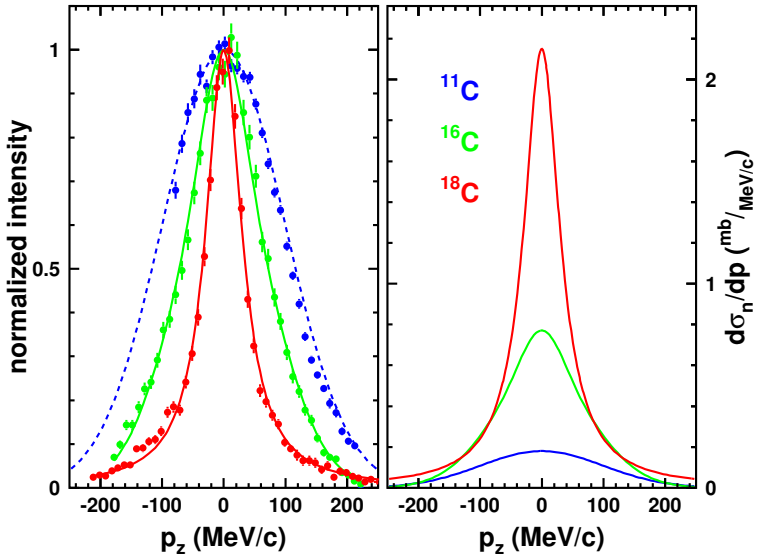

Figure 5: *Longitudinal momentum distributions of different carbon fragments, at ≈ 910 MeV/nucleon, emerging from one-neutron knockout reactions, normalised to the unit (left) and to the measured removal cross-sections. Data extracted from [28, 27].*

target, and the number of knockout residues. This last quantity is determined at the final focal plane of the spectrometer and must be corrected for the corresponding fragment transmission in the spectrometer section between the knockout target and the detection point. This transmission is evaluated by means of relatively complicated simulation programs that account for the ion-optical transport of the nuclei through the spectrometer. Other corrections, such as secondary reactions in the knockout target, detector efficiency and data acquisition dead time are also considered. The right panel of Figure 3 shows the measured momentum distributions for the different C isotopes, normalized to the corresponding cross sections. It is important to mention that in principle these two inclusive observables, core-fragment momentum distribution and nucleon removal cross section, are determined independently.

The experimental setup should also provide information on core-fragment de-excitation after knockout. The most common method for distinguishing the different core-fragment configurations contributing to the exotic nuclei wave function, which means to differentiate whether the core-fragment is in its ground state or in an excited state, is the coincident detection of the eventual core-fragment gamma- de-excitation with previously introduced observables (exclusive measurements). Therefore, the gamma-ray detector has to be located near the knockout target. Different gamma detector arrays have been used. The first experiments were performed with scintillation-based detectors (namely NaI(Tl) and CsI(Tl)) with moderate intrinsic energy resolution. In the last years they have been replaced by Ge detectors with excellent intrinsic energy resolution but considerably smaller efficiency in detecting high energy gamma-rays.

The recorded gamma-ray spectra, emitted by relativistic moving sources would be influenced by the Doppler effect (shift and broadening). The Doppler shift represents the gamma energy transformation between the laboratory and the rest reference system. The left panel in Figure 6

shows the evolution of the Doppler shift with the polar angle. For the forward angles ($\theta <$ 40 degrees), this effect significantly increases the energy in the laboratory system, which is translated into a lower detection efficiency in the gamma detector (the detection efficiency of a gamma detector depends on the gamma energy, the higher the gamma energy the lower the efficiency). Doppler broadening reflects the effect of the angular aperture of the gamma detector in the final energy resolution of the system. The right panel of Figure 6 shows the evolution of this effect with the polar angle (for a given detector angular aperture). The energy resolutions shown in this picture are calculated without considering the intrinsic energy resolution of the gamma detector used. We can also see in (Figure 6) that the Doppler shift and broadening become more dramatic as the energy of the emitter increases. The Doppler shift can be corrected by determining the velocity of the emitter and the gamma-rays emission direction. However, the broadening effect is determined by the velocity of the emitter and the detector angular aperture, and cannot be corrected. The final energy resolution will be dominated by this kinematic broadening. Thus, detector segmentation becomes a key factor, the larger the segmentation the better the energy resolution.

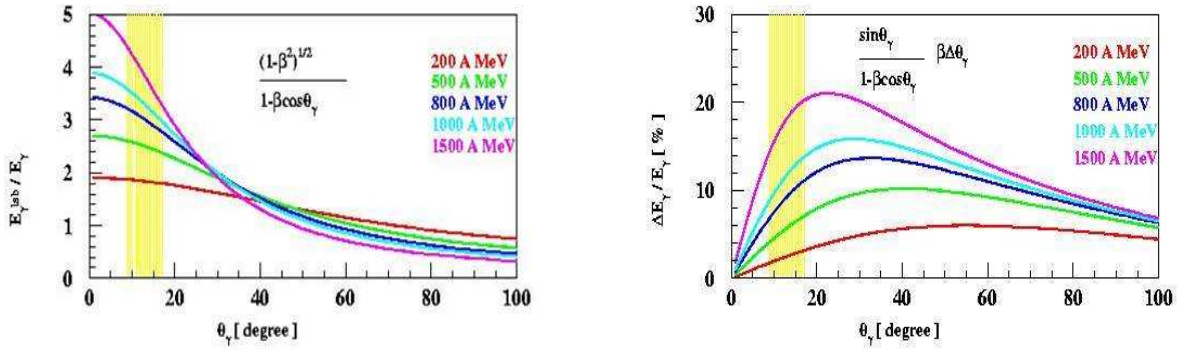

Figure 6: *Doppler shift and Doppler broadening for gamma-rays emitted by relativistic sources at different energies (curves generated for detectors with angular aperture of about four degrees).*

These "weak" points- small efficiency for energetic γ-rays and finite angular segmentation- limit the performances of gamma arrays and constitute the main uncertainty in the determination of exclusive observables. To illustrate all these effects, we see in the left panel of Figure 7 an example of a gamma detector used to perform these coincidence measurements, the MINIBALL [29] Ge array, placed at the intermediate focal plane of the FRS. The right panel of Figure 7 shows an example of a gamma energy spectra recorded in a recent experiment [31] using this detector to probe the single particle properties around ^{54}Ca (^{47}Ca here depicted was used as the reference case), where a shell closure effect for N=34 (Z=20) was predicted [30]. In this case, the emitter energy was $\approx$ 500 MeV/nucleon ($\beta \approx 1.53$). We can observe in this figure that the energy resolution achieved for the peak $\approx$ 570 keV is around a few percent. This energy resolution is considered a good result for in-beam gamma ray spectroscopy for relativistic moving sources, but it is nowhere near the intrinsic energy resolution of these Ge detectors (well below 1%).

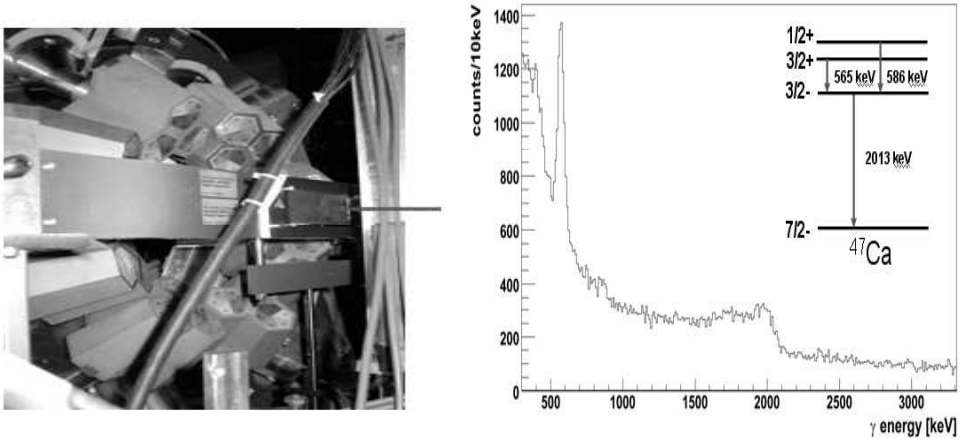

Figure 7: *Left: MINIBALL detector in its configuration at the intermediate focal plane of the FRS for recent knockout experiments. Right: Gamma-rays recorded from the* ^{47}Ca *core-fragment de-excitation following the reaction* $^{9}Be(^{48}Ca,^{47}Ca+\gamma)X$ *at around 500 MeV/nucleon [31] .*

4 Overview of experimental programs on knockout reactions

Knockout reactions have been used since the mid-1980's to investigate the nuclear structure of exotic nuclei. The first experiments focused on the study of neutron-halo states and were later extended to other exotic species. Even though this has revealed to be a very powerful method, the cases investigated concentrated on the light part of the nuclide chart. This is mainly due to the technical limitations associated with the production of secondary beams. It is important to keep in mind that the neutron dripline has only been reached for nuclei with low Z (up to Z=12). Consequently, this is where most of the knockout experiments have been performed so far.

NSCL/MSU was the first laboratory to implement the nuclear-knockout technique [32], and is still the most active in the field. For may years, knockout experiments at NSCL have focused on the study of n-rich nuclei at intermediate energies (50-150 MeV/nucleon) [1, 3]. They have also pioneered the application of the knockout technique to the study of heavier nuclei [33] and have more recently extended their experimental studies to the removal of two nucleons [7, 77, 78, 3].
In a similar energetic domain, GANIL has also applied the knockout technique on several occasions [35], whereas RIKEN has concentrated on the study of Coulomb induced breakup [71, 69]. GSI, working in a higher energetic regime (500-1000 MeV/nucleon), has carried out investigations on both Coulomb [68, 70, 72] and nuclear [28, 56, 22] knockout.

Figure 8, shows some very recent results [34] obtained at the FRS(GSI), of inclusive momentum distributions of residual nuclei after one-neutron knockout, on top of a chart of the nuclides. The vertical axis in this picture corresponds to the Z number and the horizontal axis to the N number of the exotic projectile before fragmentation. Several neutron-rich isotopes could be investigated in a single experiment where a cocktail secondary beam was produced

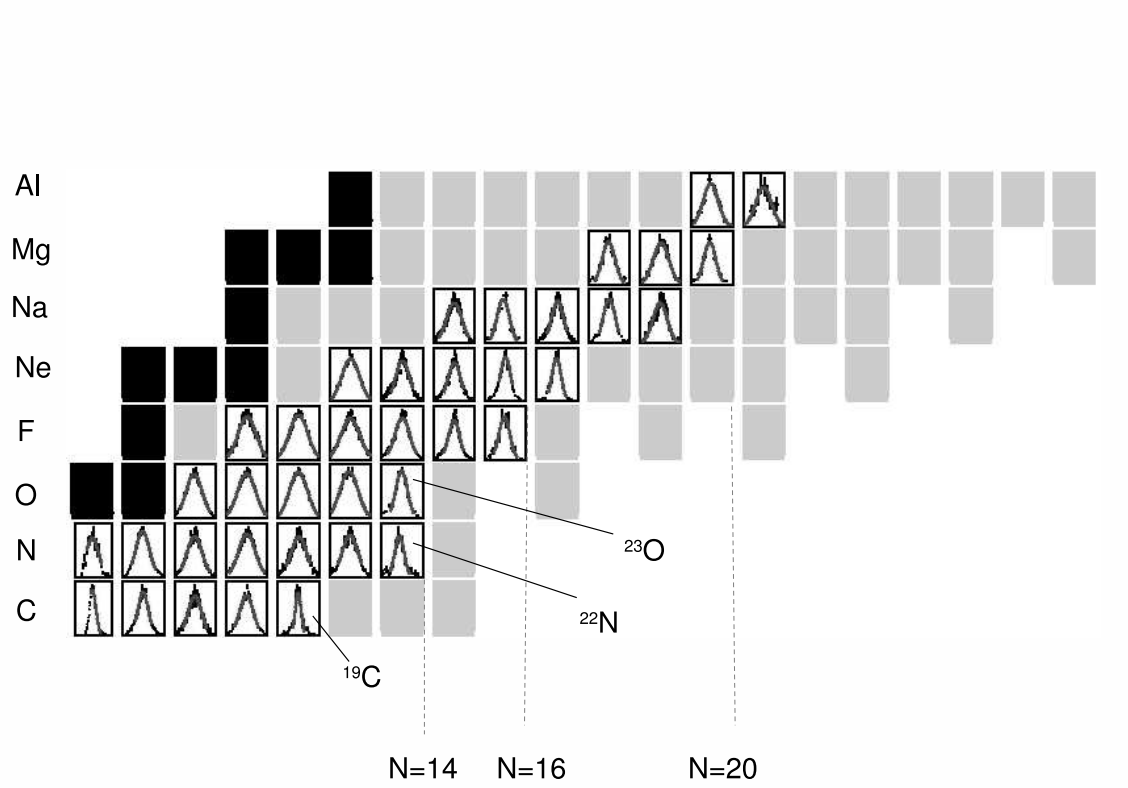

Figure 8: *Inclusive longitudinal momentum distributions of the A-1 fragments after one-neutron removal from the various projectiles indicated here on top of a chart of nuclides. Black squares correspond to stable isotopes. The measurements were performed at GSI using beam energies around 700 MeV/nucleon [34].*

by nuclear fragmentation of ^{40}Ar at 700 MeV/nucleon. Though qualitative, the evolution of the momentum distribution in this figure reflects the structural changes presented by nuclei approaching the dripline. For example one can observe the narrowness of the distribution for well known "halo states" such as ^{19}C, or the N=14 sub-shell effect (^{22}N, ^{23}O, ^{24}F, ^{25}Ne,...). This figure also reveals the potential of this technique to perform exploratory investigations, as indicated by Sauvan et al. [35], in earlier work .

The information provided by the ensemble of data obtained over at least 25 years, in different facilities and at different energetic domains is quite coherent, even though the quality is each time determined by the particular experimental conditions. For example, detection quality of the remaining fragments after knockout is excellent in experiments at higher energies, whereas the in-beam coincidence gamma detection is easier to implement at intermediate energies (see section 3 for details).

5 Halo states

Near the neutron dripline the large neutron excess and the small neutron binding energy can lead to dramatic changes in the nuclear structure. Though the years, special attention has been given to the case of nuclear halo states, where the single-particle picture provided by the shell model is unusually realistic. When approaching the driplines the separation energy of the last nucleon, or pair of nucleons, decreases gradually and the bound nuclear states come close to the continuum. In some cases, the combination of the short range of the nuclear force and the low separation energy of the valence nucleons results in considerable tunneling into the classical forbidden region and a more or less pronounced halo may be formed. A halo nuclei can be visualized as an inert core surrounded by a low density halo of valence nucleon(s) [36]. The formation of halo states is especially characteristic for light nuclei in the dripline regions, although not all of these can form a halo.

Analysis and interpretation of knockout experiments dedicated to the study of "halos" has undoubtedly led to a better understanding of the knockout technique and to its development and application as a powerful spectroscopic tool. In earlier experiments, the experimental signatures of these phenomena were the narrow momentum distribution of the emerging fragments after one-neutron knockout, this reflecting the large spatial extension of the removed nucleon, and the large one-neutron removal cross sections that constitute a complementary source for structure information (see [36] for a detailed compilation). These first experiments relied uniquely in the detection of the core-fragments and are known as "inclusive" measurements. However, we should not forget that the nuclei under study are located far away from the beta-stability line and that the resulting core-fragments are exotic nuclei themselves. As a result, core-polarisation effects are quite common. Indeed, it soon became evident that a non negligible fraction of the measured neutron-removal cross section was populating excited states in the residue. This meant that the observed longitudinal momentum distributions were in reality the superposition of broad components associated with core-fragment excited states onto the narrow distribution associated with the halo states (mainly in the core-fragment ground state).

The use of gamma-ray coincidence (described in section 3) has made it possible to separate these different contributions which in turn has made it possible to determine the partial cross-sections of the different core states. The observables extracted under these conditions are referred to as "exclusive". This exclusive experimental information, together with an adequate model describing both the structure of the nuclei involved and the reaction mechanism, allows for the experimental determination of spectroscopic factors. As we pointed out in section 3, this coincidence technique is not exempt from experimental problems. Cases involving nuclei with complex decay schemes, and/or with many weak transitions would be associated with larger experimental errors that would make a detailed analysis difficult or impossible. However, as in the case of "halos", nuclei close to the driplines exhibit very few bound states making this determination easier.

In the following paragraphs, we will concentrate on the description of two well-known cases ^{11}Be and ^{8}B, which correspond to one-neutron and one-proton halo states, respectively.

5.1 One-neutron halo ^{11}Be

Our first example is ^{11}Be with only three bound excited states and a one-neutron separation energy of $\sim$ 500 keV. The ground state of ^{11}Be, considered as a $1/2^+$ intruder from the *sd* shell, is a well known one-neutron halo state. First experimental evidences came from the

measurement of the half-life of the 320 keV excited state of ^{11}Be, suggesting an extremely strong E1 transition [38], and the narrow momentum distribution of ^{10}Be core-fragments resulting after one-neutron knockout of ^{11}Be [39]. The naive picture of an inert ^{10}Be core and a neutron in a $1s$ shell, soon gave way to a more complex picture where the pertinence of this inert core was questioned.

The most favourable scenario consisted of an admixture of a neutron in a $0d_{5/2}$ coupled to the first excited state in ^{10}Be (2^+), but theoretical predictions ranged in their estimates from 7% to 40% [43, 44]. The experimental situation was ambiguous, with different results from a ^{10}Be(d,p)^{11}Be experiment providing quite different spectroscopic factors [45, 46, 47], some of them incompatible with earlier Coulomb dissociation experiments [48, 49]. The knockout experiment performed by T. Aumann et al. [37] at NSCL (A1900/S800) shed light on this question. They produced a secondary beam of ^{11}Be at 60 MeV/nucleon by nuclear fragmentation of ^{16}O. The ^{11}Be beam impinged on a Be target producing the one-neutron knockout. A NaI(Tl) array located around the removal target recorded the gamma-rays in coincidence with the ^{10}Be fragments, which were analysed with the tracking detectors located at the end of S800 (see experimental details in [37]). The resulting gamma-energy spectrum is displayed in the left panel of Figure 9, where the solid line represents a fit to the experimental spectrum. The different gray lines correspond to a Montecarlo simulation of the individual decay lines. The gamma-rays facilitated the experimental determination of partial cross-sections that are

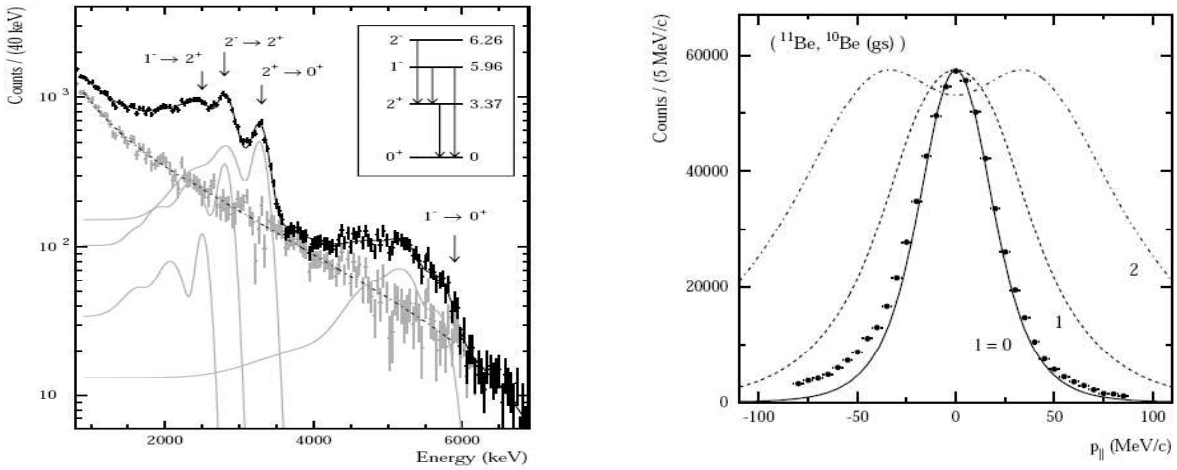

Figure 9: *Left: Doppler-corrected gamma energy spectrum measured with the NaI array in coincidence with ^{10}Be core-fragments emerging from the ^{9}Be(^{12}Be,^{11}Be+γ)X one-neutron knockout. Right: Longitudinal momentum distribution of the ^{10}Be ground state fragments. The curves are calculations assuming a knockout reaction from s, p, and d states [37].*

summarised in table 1. The calculations shown in this table correspond to single-particle cross sections in the spectator-core eikonal three-body model. They are given separately for knockout (stripping) and diffractive breakup. The theoretical cross-section for a given ^{10}Be core final state and the removed nucleon j value, is assumed to be the product of a spectroscopic factor (C^2S) [50] and a single-particle cross section, which is the sum of the different contributions mentioned above. This theoretical cross section is then compared with the experimental values, allowing us to test the picture provided by the reaction mechanism description and the nuclear structure (spectroscopic factors calculated within the shell model), to determine how realistic

Table 1: *Partial cross sections (mb) to all final states I^p observed in ^{10}Be after one-neutron knockout from ^{12}Be. Different contributions of theoretical single-particle cross sections in the eikonal model are reported. The sum multiplied by the spectroscopic factor is compared with the experimental values [37].*

I^π	l	CS	σ_{sp}^{knock}	σ_{sp}^{diff}	σ^{other}	σ^{theo}	σ^{expt}
0^+	0	0.74	125	98	10	172	203(31)
2^+	2	0.18	36	14	11	17	16(4)
1^-	1	0.69	25	9		23	17(4)
2^+	1	0.58	25	9		20	23(6)
Σ						224	259(39)

it is. Table 1 shows a quite good agreement between the experimental results and theoretical calculations. This result also corroborates a dominance of s-wave single particle configuration for the ground-state.

With this experimental setup, it was possible to discriminate the ground-state from the other excited states for the ^{10}Be fragment momentum distribution. The results are shown in the right panel of Figure 9, together with calculations assuming a knockout reaction from s, p and d neutrons. Here we see that the narrow momentum distribution (FWHM = 47.7(6) MeV/c), associated with the ^{10}Be g.s, is only compatible with the case of nucleon removal from a $1s$ state. The momentum distributions for the excited states are consistent for the 6.0 MeV gamma-ray with the known $p_{3/2}$ core state assignment, while the momentum gated on the $2^+ \rightarrow 0^+$ transition (3.4 MeV) contains contributions from both p and d neutrons. This experiment was then very successful in determining the ground state structure of ^{11}Be, quantifying the admixture of the ^{10}Be excited core to it. It provided a good understanding of the reaction mechanism and structure of the nuclei involved.

5.2 One-proton halo ^8B

Another interesting case is ^{8}B. With one bound state and a one-proton separation energy of 137 keV, ^{8}B is the only known nucleus with a proton halo structure in its ground state. Experimental evidence for it was seen in earlier measurements of a large one-proton removal cross section of 98 ±6 mb (on carbon) and a narrow longitudinal momentum distribution of 93 ± 5 MeV/c [51, 52, 53].

Because it is an $A = 8$ nucleus, reactions involving ^{8}B are important to understand how the nucleosynthesis bridges the $A = 8$ mass gap. In particular, the astrophysical interest in ^{8}B stems from its key role in the production of high-energy solar neutrinos [54]. The need for accuracy in this number has not diminished after the reports on neutrino oscillations [55]. Indeed, the proton capture rate of ^{7}Be strongly depends on the structure of ^{8}B.

When describing ^{8}B as a one-proton halo system, one should keep in mind that the ^{7}Be core is itself a weakly bound system, which can be considered as a two-body system (^{4}He + ^{3}He). The ^{7}Be $3/2^-$ ground state is bound by 1.587 MeV, and the only bound state below the α+^{3}He threshold is the $1/2^-$ state at 429 keV excitation energy. If ^{8}B is treated as a two-body system, there are three possible ways to couple a proton to the ^{7}Be core: the last proton in ^{8}B can be in either a $p_{3/2}$ or a $p_{1/2}$ state, and the possible ground state configurations of ^{8}B (I^π=2^+) thus are:

a) $\psi\big(\,^{7}\mathrm{Be}(3/2^{-})\big) \otimes \psi\big(\mathrm{p}(3/2^{-})\big)$
b) $\psi\big(\,^{7}\mathrm{Be}(3/2^{-})\big) \otimes \psi\big(\mathrm{p}(1/2^{-})\big)$
c) $\psi\big(\,^{7}\mathrm{Be}(1/2^{-})\big) \otimes \psi\big(\mathrm{p}(3/2^{-})\big)$

An experiment was performed at the FRS (GSI) [56] with a ^{8}B beam at 936 MeV/nucleon, produced by nuclear fragmentation of a ^{12}C primary beam. This ^{8}B beam impinged on a C target located at the intermediate focal plane of the FRS. Fragment longitudinal momentum distributions after proton knockout and the cross section of the process were determined in the experiment. An array of NaI(Tl) detectors, located close to the knockout target and covering the forward direction, allowed the coincidence measurement of the 429 keV γ rays. Tracking detectors located at the final focal plane determined the momentum distribution of the ^{7}Be fragments after one-proton removal process of ^{8}B. This coincidence measurement provided direct information about the contribution from configuration (*c*) to the ^{8}B ground state wave function.

The gamma-rays recorded in the experiment are presented in the left panel of Figure 10. A summary of the experimental results achieved is also shown in Table 2. The theoretical values were obtained using the eikonal approximation with a three body model (^{4}He+^{3}He+t) to describe the ^{8}B wave function.

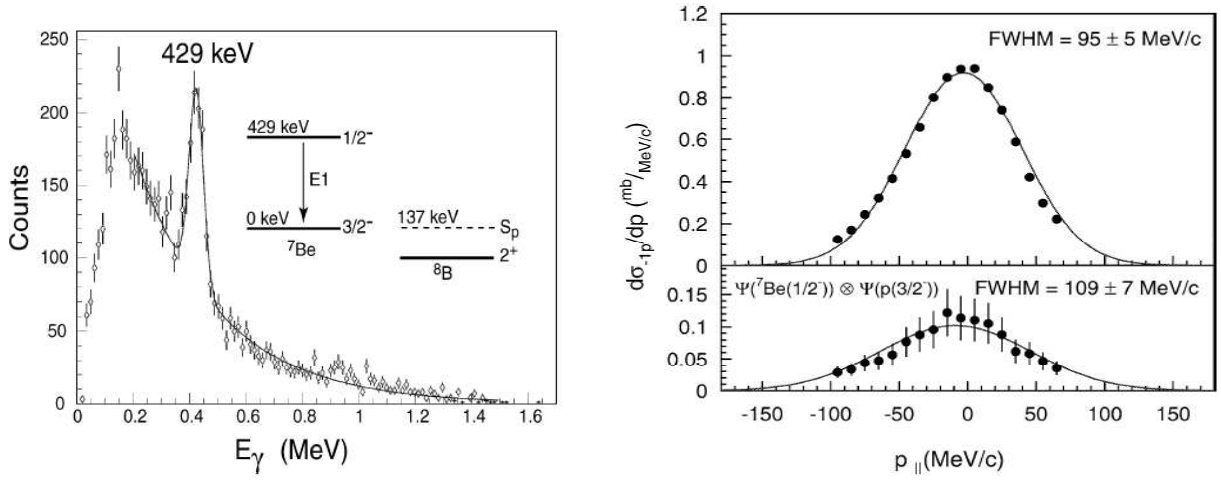

Figure 10: *Left: Energy spectrum of γ rays after Doppler correction in coincidence with ^{7}Be fragments after one-proton removal reactions of ^{8}B in a carbon target. Right: (top) Inclusive and (bottom) exclusive $p_{\|}$ momentum distribution of ^{7}Be core-fragments emerging from the $^{12}C(^{8}B,^{7}Be+\gamma)X$ one-proton knockout. Exclusive data refer to contributions in coincidence with the 429 keV state in ^{7}Be. In both cases, the full curve represents the theoretical calculation folded with the experimental resolution and scaled to match the amplitude of the experimental spectrum. The widths of these curves are 99 and 130 MeV/c respectively [56].*

The gamma coincidence also allowed to discriminate the fragment longitudinal distribution involving configuration (*c*) from the others. In this case the removed protons are always in a *p* state as shown the right panel of Figure 10, and no appreciable difference in the fragment momentum distribution width is observed.

The ratio of the cross section of ^{7}Be in its excited state to the total cross section is found to be 13±3 % which is in excellent agreement with the theoretical value of 14 %. This indicates

Table 2: *Comparison between theoretical and experimental results for inclusive and in coincidence, one-proton removal cross sections and $p_{\parallel}$ (FWHM) after one proton removal of ^{8}B. The theoretical widths in this table include the experimental resolution.*

	σ_{-1p} (mb) exp.	σ_{-1p} (mb) theo.	$p_{\parallel}$ (MeV/c) exp.	$p_{\parallel}$ (MeV/c) theo.
total	94 ±9	82	95±5	99
excited	12±3	11.5	109 ±7	130

that the $\psi(\,^{7}\mathrm{Be}(1/2^{-})) \otimes \psi(\mathrm{p}(3/2^{-}))$ component in the ^{8}B ground state wave function has a significant weight of about 16%. The ratio between the experimental and theoretical cross section indicates how realistic the "prescription" used in the used model is. This will be explained later in section 6.1. Based on this the results for ^{8}B shown an excellent agreement with the calculations, indicating the good quality of the reaction mechanism description and ^{8}B nuclear structure used, as we saw for ^{11}Be.

6 Knockout reactions as general purpose spectroscopic tool

6.1 Determination of spectroscopic factors

We saw in section 5 that knockout reactions are able to determine the nuclear structure of weakly bound halo states. The question now is whether this technique can be applied to the study of other exotic species. I would like to introduce the discussion by illustrating it with another example: that of ^{23}O [22] studied by neutron-knockout at relativistic energies (939 MeV/nucleon) at the FRS-GSI. ^{23}O, with a neutron separation energy of 2.7 MeV, lies very close to the dripline and has no bound excited states below 4 MeV [57]. In the nuclide chart, it is surrounded by ^{22}O (A-1 core-fragment), with a first excited 2^{+} level at 3.17 MeV and ^{24}O (dripline) with no excited states below 4 MeV [57]. Both neighbors seem to be double magic nuclei, indicating a persistence of the proton-magic shell at Z=8 and (sub-) shell closures at N=14 and N=16. Previous experimental work on this nucleus yielded contradictory results concerning spin and parity assignment for the ground state of ^{23}O [35, 58], which motivated a deeper investigation of this nucleus. The experimental measurement of the core-fragment momentum distribution and gamma-rays in coincidence was performed with the same experimental setup as the case described for ^{8}B. The left panel of Figure 11 shows the energy spectrum of gamma-rays recorded in coincidence with the ^{22}O fragments. This gamma spectrum was used to determine the exclusive cross section for different final core-fragment states. The broad peak observed at higher energy is assumed to be due to the 3.2 MeV and the 2.6 MeV transitions that the NaI(Tl) detectors could not resolve. The exclusive momentum distributions were extracted assuming that all ^{22}O excited levels decay through the first excited state at 3.2 MeV. This peak was, therefore, used to gate the longitudinal momentum distribution in order to obtain the exclusive momentum distribution of the ^{22}O ground state (Figure 11 right). Comparison of the momentum distribution involving ^{22}O in its g.s with calculations performed within the eikonal approximation, assuming angular momenta $l = 0$ and $l = 2$, and in particular the agreement with the case $l = 0$, favoured the configuration of a $2s_{1/2}$ neutron coupled to the $^{22}\mathrm{O}(0^{+})$ core.

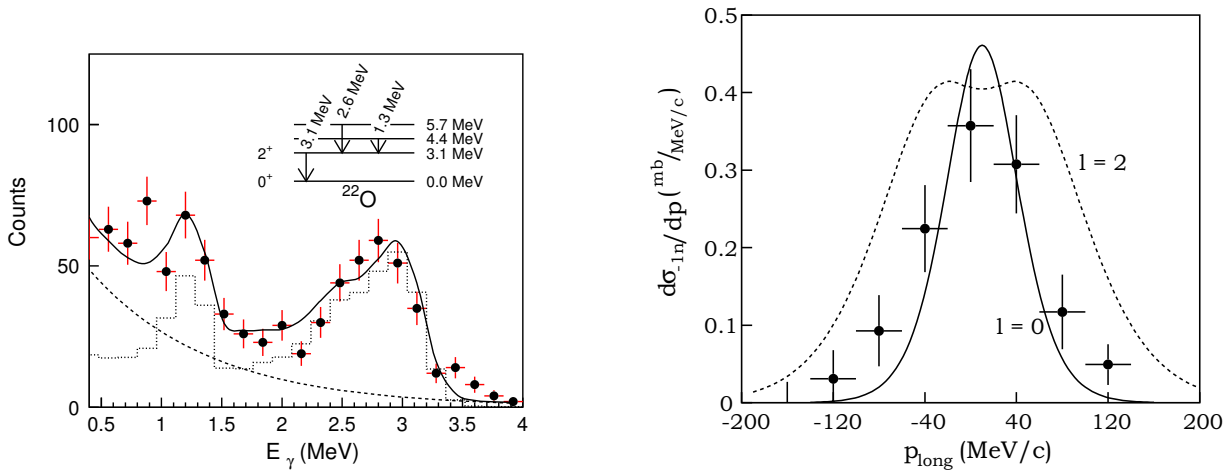

Figure 11: *Left: Spectrum of γ rays in coincidence with ^{22}O fragments after one-neutron removal from ^{23}O in a carbon target. The spectrum shown here has been obtained from the measured γ-ray spectrum after Doppler correction. The experimental spectrum is compared with the result of a GEANT simulation adopting the level scheme shown above. Right:Ground-state exclusive momentum distribution for ^{22}O fragments after one-neutron knock-out reaction from ^{23}O compared with calculations assuming $l = 0$ and $l = 2$*

This agreement also led us to conclude that the ground-state spin of ^{23}O is $I^\pi = 1/2^+$ which brought the experimental controversy to an end.

Using the eikonal approach [59], one-neutron removal cross sections were also obtained for the individual single-particle configurations. For the neutron knockout from the $2s$ shell the calculated cross section is 51 mb, in agreement with the experimental value of 50±10 mb. This result confirms the large spectroscopic factor for the s-neutron ($C^2S = 0.8$) obtained by shell-model calculations [60]. The knockout of a neutron from the $1d$-shell in this calculation results in ^{22}O either in the 2^+ state (20.0 mb), or in the 3^+ state (18.3 mb). The contribution of neutron knockout from deeper p shells ($1^-, 0^-$ states) amounts to 15 mb. Comparison of these experimental data with theoretical predictions shows that the contribution of excited states is significantly smaller. The discrepancy might be related to the experimental errors associated with the extraction of exclusive observables (mainly the gamma-ray detector), or the deficiencies of the relatively simple single-particle model that was used.

Table 3: *Comparison of measured and calculated cross-sections and spectroscopic factors for $^{12}C(^{23}O,^{22}O+\gamma)X$ one-neutron knockout [22].*

E (MeV)	I^π	σ_{sp} (mb)	$\sigma_{exp.}$ (mb)	$S_{exp.}$	C^2S [60]
0	0^+	51	50±12	0.97(23)	0.80
3.2	2^+	20	10.5±2.6	0.52(23)	2.13
4.5	3^+	18	14±4	0.77(23)	3.08
5.8	1^-,(0^-)	15	10.5±2.6	0.7(23)	0.85(0.33)
	Sum	104.5	85±15		

Further investigations of these findings are certainly needed and take us back to the question at hand: To what extent can knockout reactions be used to determine spectroscopic factors? A few decades ago, various methods were used to experimentally determine the spectroscopic factors in stable nuclei. One of them, was nucleon transfer, which exhibits a high sensitivity to single-particle components in the wave function. This method is also used today with unstable nuclei. Another method consists of using quasi-free reactions such as (p,2p), induced by high energy proton beams, to excite deep-hole states. These reactions also gave us access to the associated single-particle properties.

However, the "cleanest" method is the quasi-free "proton knockout" using high energy electrons (e,e'p), that allows us to determine the spectroscopic factors of proton single-particle states [4, 61, 5]. It is very interesting to note that these investigations found that the measured spectroscopic factors for deep-hole proton states over quite a large nuclear mass range, were lower by a factor 0.5-0.6 than those calculated by the shell model. Indeed, the term of "knockout reactions" as it refers to nucleon removal or breakup was inspired from reactions of this kind. P.G. Hansen and J.A. Tostevin [1] analysed how well the spectroscopic factors deduced from several partial knockout cross sections in the $p - sd$ shell (measured for most cases at NSCL), compared with spectroscopic factors estimated by shell model calculations. Figure 12 shows that the results agreed very well in general. However it is possible to identify cases that do not follow the general trend, such as the core-excited states in ^{23}O neutron-knockout.

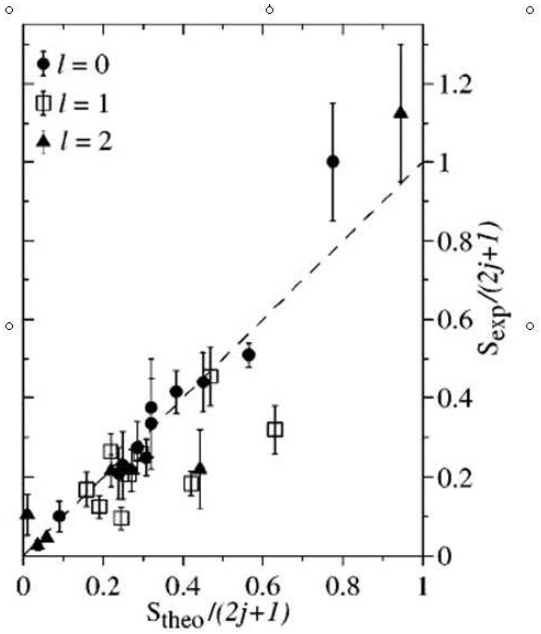

Figure 12: *Experimental versus theoretical spectroscopic factors in units of the sum-rule value (2j + 1). The dashed line is the diagonal. Both quantities show a correlation with a scale factor close to one [1].*

The diagonal in Figure 12 shows the correlation between experimental and theoretical spectroscopic factors with a scale factor close to one. It is interesting to notice that the points clearly lying bellow this correlation line correspond to high energy excited states. This seems

to be connected to the quenching of the spectroscopic factors observed two decades ago in (e,e'p). These observations were further investigated by Tostevin et al. [62]. Figure 13 summarises these investigations and confirms the existence of a quenching or empirical reduction factor of spectroscopic factors (R_s), defined as the ratio between experimental and theoretical exclusive cross sections. This picture is a compilation of experimental results from quasi-free "proton knockout" using high energy electrons (e,e'p), along with proton and neutron knockout. It shows the dependence of the quenching factor with the difference between the proton and neutron separation energy (ΔS). Is interesting to note that the physical occupancies are

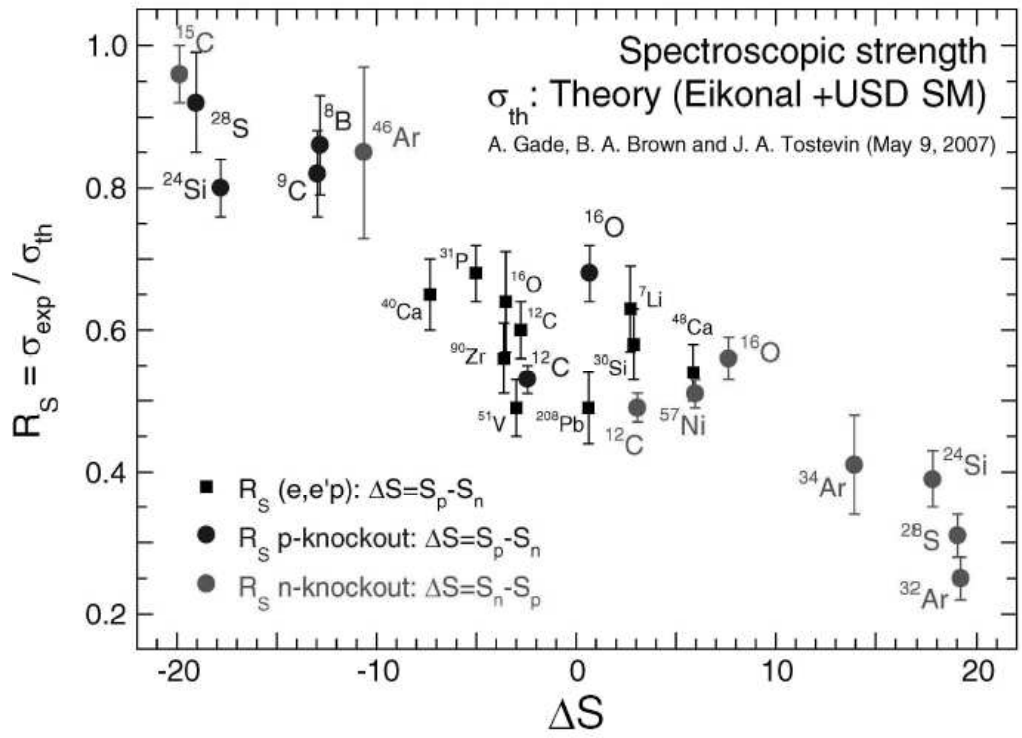

Figure 13: *Summary of quenching or empirical reduction factor obtained for spectroscopic factors evaluated from knockout reactions[62].*

in general much lower than those suggested by the shell model, however this discrepancy is smaller for loosely bound nuclei (≈ 0.85 left top corner in Figure 12). Cases corresponding to proton-removal, with values ranging from 0.5 to 0.6, are in agreement with the findings obtained earlier with quasi-free "proton knockout" (e,e'p) reactions. Knockout of deeply bound nucleon (right bottom corner in Figure 12) is associated with R_s factors lower than 0.4. Using (e,e'p) [63] as an analogy again, this small reduction factor is interpreted in terms of correlation effects that reveal the simplified picture of nuclei provided by effective-interaction theories such as the shell model. Measurements of absolute nucleon occupancies, such as those provided by both quasi-free "proton knockout (e,e'p) and nucleon removal reactions would help to quantify these correlation effects.

To complete the picture, note that Figure 13 contains a mixture of exclusive and inclusive information. In the inclusive knockout cross section the quenching factor R_s is defined as the ratio of the experimental cross section to the sum of the theoretical cross sections to any state lying below the neutron threshold.

We will complete this overview with some details about the experimental study of ^{32}Ar [64] via one-neutron knockout at 61 MeV/nucleon, probably the most bound case investigated so far with this technique, which leads to the proton-dripline nucleus ^{31}Ar. This nucleus, with a $5/2^+$ ground state is peculiar because it has no bound excited states. Direct measurement of the core-fragment provides exclusive information without need of gamma coincidence.

From the experimental point of view there is an important difference between this experiment and all the others previously discussed. The S800 spectrograph was operated in "focus mode" with larger acceptance but lower intrinsic momentum resolution, as shown in Figure 14. The theoretical momentum distributions depicted in this figure were calculated using the black-

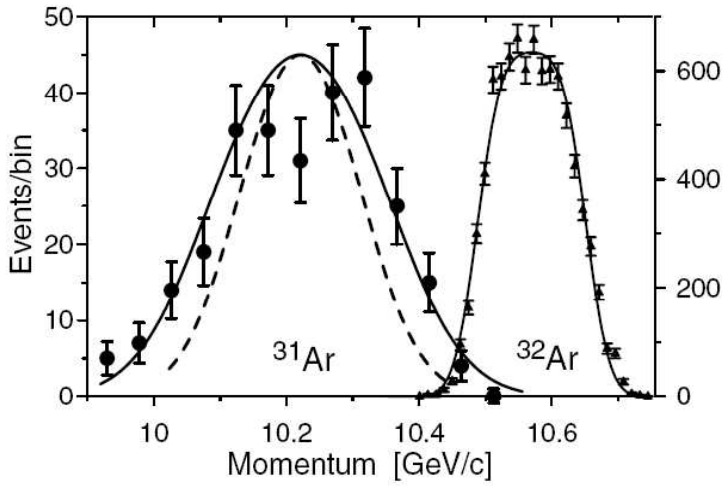

Figure 14: Longitudinal momentum distribution of ^{31}Ar residues after one-neutron knockout reaction, compared with theoretical calculations assuming l=0 (dashed line) and l=2 (solid line) knocked-out neutrons. The unreacted projectile beam ^{32}Ar fitted with a rectangular distribution folded with a Gaussian resolution function is also shown. [64].

disk model [1] and folded with the measured response of the apparatus. This spectrum clearly associates the reaction with a l=2 knockout neutron, confirming the spin and parity assignment for the ^{31}Ar ground state of $5/2^+$. Comparison of the experimental cross section 10.4(13) mb with the theoretical one yields a surprisingly low quenching factor of 0.24(3). The authors of this work compared this case with ^{22}O, which has the same neutron number N=14 and Z=8 protons, and considered as almost doubly magic nucleus. The quenching factor, R_s, obtained in this case is 0.70(6) (using an average of two different experimental results [35, 22] as experimental cross section), which is well above the result obtained for ^{32}Ar. The authors suggested that this very strong quenching indicates nuclear structure effects, reflecting correlations linked to the high neutron separation energies (22.0 MeV) in very asymmetric nuclear matter.

In spite of such significant experimental and theoretical progress, much remains to be understood. The determination of absolute spectroscopic factors with nucleon removal reactions induced by radioactive beams will undoubtedly be a topic of discussion in coming years.

6.2 Comparison with Coulomb dissociation experiments

Coulomb induced one-neutron removal has also been widely used [68, 69, 70, 71, 72] as spectroscopic tool in a way quite similar to the nuclear case addressed in this lecture. In this case,

the observable that provides the spectroscopic information is the dipole-strength distribution, extracted from the differential cross-section for the electromagnetic excitation, which can be calculated using the semi-classical approximation described in [65, 66, 67].

The interesting task of comparing spectroscopic factors determined by both methods was undertaken by T. Aumann [2]. Figure 15 summarises the main results obtained for the $2s_{1/2}$ halo states, using both methods in different experiments at various energies. Squares represent data obtained in the energy regime 50-100 MeV/nucleon whereas circles correspond to energies between 0.4- 1 GeV/nucleon. Open symbols correspond to results deduced from nuclear knockout and filled symbols represent cases of Coulomb-induced knockout. The results show the consistency of the experimental methods used. Different model analyses yield spectroscopic factors within 10-20%. No clear systematic difference could be observed except that spectroscopic factors deduced by Coulomb dissociation are slightly lower than the others.

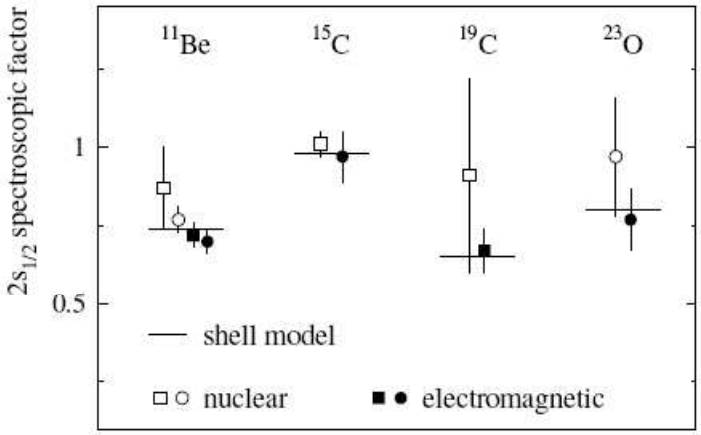

Figure 15: *Spectroscopic factors of $s_{1/2}$ halo states, investigated by nuclear and Coulomb breakup. Squares represent data obtained in the energy regime 50-100 MeV/nucleon whereas circles correspond to energies between 0.4- 1 GeV/nucleon. Open symbols correspond to results deduced from nuclear knockout and filled symbols represent cases of Coulomb-induced knockout[2].*

6.3 Bench mark of nuclear structure models

In section 6.1, we observed the important role that nucleon knockout plays in the experimental determination of absolute spectroscopic factors. We also mentioned that the difficulty of determining these quantities increases significantly as we move farther away from the nucleon dripline, with core fragments exhibiting an important number of possible final states.

However, it is important to stress that even in these complex cases the nucleon-knockout technique has proven to be very useful in providing structural information. An example of this is the neutron- knockout of ^{28}Ne [73]. This experiment was performed at NSCL with a secondary beam of about 80 MeV/nucleon using a segmented Ge configured in nine angle pairs ranging from 24^o to 147^o. Figure 16, left, shows three gamma-rays at 0.119, 0.765, and 0.885 MeV, recorded from the ^{27}Ne de-excitation. The 0.119 and 0.765 MeV gamma-rays were found to be in coincidence, suggesting that only two excited states were populated, as shown in the inset of this figure, and confirming previous work [74].

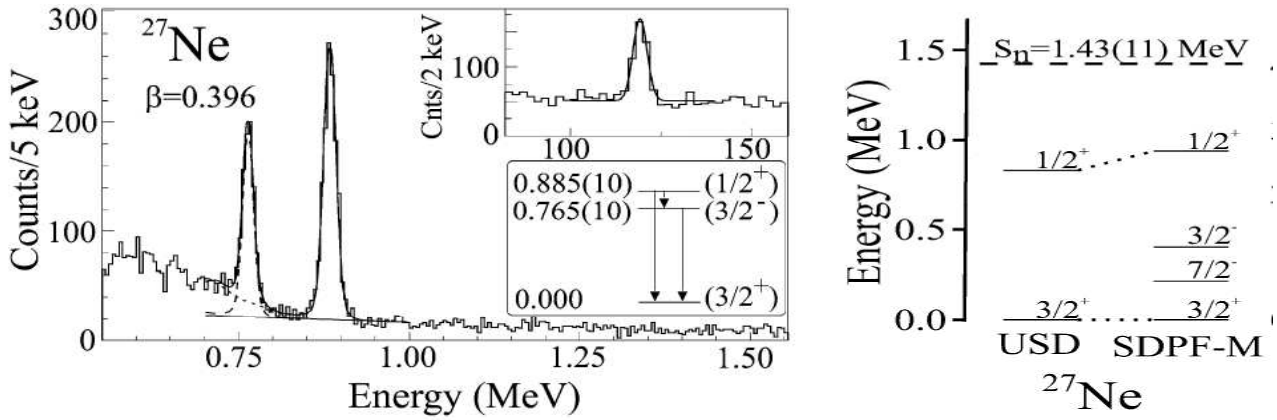

Figure 16: *Left: Doppler-reconstructed gamma-ray energy spectra from single- neutron removal from ^{28}Ne. Right: Bound states predicted for ^{27}Ne by USD and SDPF-M calculations. [73].*

The exclusive longitudinal momentum distributions were obtained by applying the coincidence method. Both ^{27}Ne excited states were associated with removed neutrons with l=0 or l=1 but the large experimental errors frustrated hopes for a definitive assignment. The momentum distribution of ^{27}Ne ground sate was significantly broader, but quantitative interpretation was not possible.

Figure 16, right, shows two different shell-model calculations for ^{27}Ne. Both models give very different predictions for the neutron-rich Ne isotopes, which are located in a transitional region between N = 16 and N = 20. Conventional calculations performed with the Universal SD (USD) interaction with a limited configuration space, do not allow for intruder configurations across the N = 20 gap, and thus fail to reproduce shell-breaking effects near N = 20. SDPF-M calculations indicate that intruder configurations are important for ^{27}Ne (N = 17), even in the low-lying level scheme. On the other hand, SDPF-M predictions in this transitional region compare well with known level structures and electromagnetic moments.

What is interesting here is that the ^{27}Ne measured gamma rays show the presence of low-lying states and thus contradict the USD shell model, which predicts only one bound excited state, and are consistent with the SDPF-M shell model calculations.

Further analysis in terms of exclusive cross-sections was also carried out by the authors, who calculated single particle cross sections in the three-body reaction model [59]. The ratio of experimental and single particle cross sections made it possible to determine experimental spectroscopic factors. However, spectroscopic factors from the SDPF-M model were not yet available, providing only an upper limit, in quite good agreement with the experimental spectroscopic factors.

This experiment reports direct evidence of population of the $3/2^-$ intruder state in ^{27}Ne in the knockout of a single neutron from the ground state of ^{28}Ne. There are two important implications to this experimental finding; first, that this low-lying negative parity state is consistent with a narrower shell gap for exotic nuclei with Z$\ll$N and N$\approx$20; second, it clearly favoured Monte Carlo shell-model calculations with the modern SDPF-M interaction that successfully describe neutron-rich nuclei in the vicinity of N = 20, where normal and intruder configurations coexist at low excitation energy.

Consequently, this example demonstrates the general importance of direct reactions and particularly nucleon-knockout for the study of exotic nuclei. It is a bench-mark experiment in the predictive power of large-scale shell-model calculations.

7 Two nucleon removal

A few years ago, the panorama of "direct reactions" induced by exotic beams was enlarged by Bazin and collaborators [7], who suggested the two-proton removal of very neutron-rich nuclei as a single step direct reaction.

It is based on the idea that the competing two-step process of a first proton-knockout followed by a proton evaporation is strongly suppressed in comparison with the neutron evaporation from the neutron-rich intermediate state, which is shown in Figure 17 (extracted from in [75]). Later on, the two-neutron knockout from neutron-deficient projectiles was shown to be a direct process as well. There has been rather intense activity around this topic during the last years in the NSCL community, in both experimental [7, 77, 78, 79] and theoretical [75, 76] aspects (see also review articles [1, 3]).

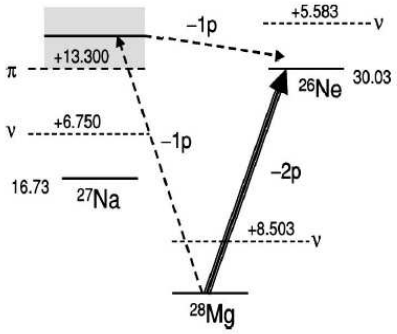

Figure 17: *Energy diagram of the neutron-rich N=16 isotones (^{28}Mg, ^{27}Na, and ^{26}Ne), illustrating that direct population of the bound states of 26Ne from ^{28}Mg, is favoured over the two step process of one-proton removal to excited ^{27}Na followed by proton evaporation[75].*

The inclusive cross-section of the two-nucleon knockout process is significantly smaller than the corresponding one-nucleon process, reaching maxima of only a few mb. Even though the cross-sections are small, interesting results have already been obtained. Among these are experimental observables with inclusive momentum distribution for the emerging fragment and the associated cross-sections (both inclusive and exclusive). The inclusive residue (projectile minus two nucleons) momentum distributions obtained so far do not allow us to extract quantitative spectroscopic information. Investigations of this kind will certainly increase in the near future.

It is also important to emphasize the developments in the description of the reaction mechanism for the two-nucleon knockout process. Early work by Bazin and collaborators [7] included a simplified model where the two removed nucleons were uncorrelated and diffractive processes were completely neglected. In its present form, the description includes ingredients of eikonal reaction theory and correlated many-body wave functions from shell-model calculations. With these considerations, the cross-section of the two-nucleon removal process is expressed as (to compare with equation 2 for one-nucleon knockout)

$$\sigma_{sp} = \sigma_{str} + \sigma_{str-dif} + \sigma_{dif} \tag{7}$$

where σ_{str} and σ_{dif} correspond to events where both nucleons are either absorbed or elastically scattered respectively, and $\sigma_{str-dif}$ corresponds to one nucleon absorbed by the target, while the other scatters elastically (details on the reaction model can be found in [75, 76]).

The strong effect of including correlations in the reaction mechanism description is shown in Figure 18 which presents the result of ^{9}Be(^{28}Mg,^{26}Ne+γ)X two -proton knockout cross-sections to individual final states of ^{26}Ne and compares it with calculations of correlated and uncorrelated protons

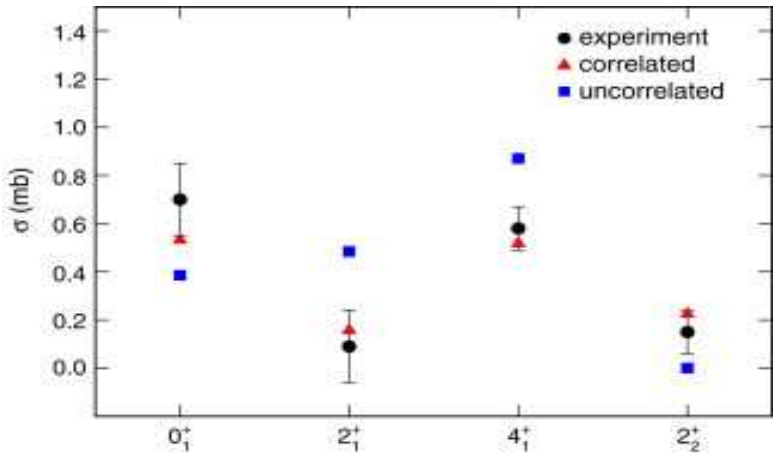

Figure 18: *Cross-sections of individual final states(circles) in the two-proton knock-out reaction[7], compared with the corresponding theoretical cross-section [76] for correlated(triangles) and uncorrelated(squares) protons (figure extracted from [3]).*

8 Summary

We have presented in this lecture the interesting implications of using "knockout reactions" as an appropriate technique for investigating the nuclear structure of exotic nuclei. The aim of this lecture was also to emphasize the experimental and conceptual aspects associated to these kind of experiments and their possible ramifications in the analysis and interpretation of the results. Theoretical aspects of the method are subject of Daniel Baye's lecture (in this school).

Halo nuclei, which have a relatively simple and well-known nuclear structure, were used to show the power of the method. Experiments of one-nucleon knockout from halo states provide a very satisfactory description of the reaction mechanism, making it possible to experimentally deduce the structure of the involved nuclei.

Though generally successful, application of the technique to more complex nuclei, is not without experimental "difficulties" that complicate the extraction of quantitative information. Reactions of this kind have been used to measure the physical occupancies (C^2S) associated with the different configurations that define the ground state of the exotic nuclei under study. The experimental spectroscopic factors obtained are generally smaller than those predicted by the large-scale shell model. The existence of these quenching factors has been interpreted in terms of correlation effects pointing out the simplified picture of nuclei provided by shell model calculations. The technique has also proven useful for bench-marking different structure models.

Even though great progress has been made, the situation is not yet clear and the determination of absolute spectroscopic factors with nucleon removal reactions induced by radioactive beams will certainly be a hot topic in the next years. The relatively recent extension of the technique to the study of two-nucleon removal looks promising, though it has not yet provided quantitative information. This will also be a subject for investigation in coming years.

Construction of new generation facilities (i.e: NUSTAR/FAIR, BIGRIPS and NFS), in the near future, will significantly increase the intensity of the available exotic beams. This, together with the development of new specific detection systems (i.e : R3B@NUSTAR/FAIR) will open new perspectives in this field.

References

[1] P.G. Hansen and J.A. Tostevin, *Direct Reactions with Exotic Nuclei*, Annu. Rev. Nucl. Part. Sci. **53** (2003) 219.

[2] T. Aumann, *Reactions with fast radioactive beams of neutron-rich nuclei*, Eur.Phys.J. **A26** (2005) 441.

[3] A. Gade and T. Glasmacher, *In-beam nuclear spectroscopy of bound states with fast exotic ion beams*, Prog. Part. Nucl. Phys. **60**(2008) 161

[4] V.R. Pandharipande, I. Sick, P.K.A. de Witt Hubers, *Independent Particle Motion and Correlations in Fermion Systems*, Rev. Mod. Phys. **69** (1997) 981.

[5] G.J. Kramer, H.P. Blok and Lapikas, *A Consistent Analysis of (e, e'p) and (d, 3He) Experiments*, Nucl. Phys. **A679** (2001) 267.

[6] D. Warner, *It is a knockout*, Nature **425** (2003) 570.

[7] D. Bazin et al., *New Direct Reaction: Two-Proton Knockout from Neutron-Rich Nuclei*, Phys. Rev. Lett. **91** (2003) 012501.

[8] P.G. Hansen, *Studies of Single-Particle Structure at and Beyond the Drip Lines*, Nucl. Phys. **A 682** (2001) 310

[9] W. Catford, *Nucleon transfer via (d, p) using TIARA with a* ^{24}*Ne radioactive beam*, Jour. Phys. **G31** (2005) S1655

[10] I. Tanihata et al., *Measurements of Interaction Cross Sections and Nuclear Radii in the Light p-Shell Region*, Phys. Rev. Lett. **55** (1985) 2676.

[11] I. Tanihata, *Research opportunities with accelerated beams of radioactive ions*, Nucl. Phys. **A 693** (2001) 1.

[12] J.S. Al-Khalili et al. *Evaluation of an eikonal model for* ^{11}*Li-nucleus elastic scattering* , Nucl. Phys. **A 581** (1995) 331.

[13] T. Kobayashi et al., *Projectile fragmentation of the extremely neutron-rich nuclei* ^{11}*Li at 0.79 GeV/nucleon*, Phys. Rev. Lett. **60** (1988) 2599.

[14] R.J. Glauber, *Lectures in theoretical physiscs*, ed WE Brittin, New York, Interscience (1954).

[15] Gottfried K., *Quantum Mechanics, p. 113*, New York: Benjamin (1966)

[16] P. G. Hansen, *Momentum content of single-nucleon halo*,Phys. Rev. Lett. **77** (1996) 1016.

[17] H. Esbenssen, *Momentum distributions in stripping reactions of single nucleon halo nuclei*, Phys. Rev. **C 53** (1996) 2007.

[18] J. Tostevin, *Single-nucleon knockout reactions at fragmentation beam energies* Nucl. Phys. **A 682** (2001) 320.

[19] H. Esbensen and G.F. Bertsch, *Eikonal Approximation in Heavy-Ion Fragmentation Reactions* , Phys. Rev. **C 64** (2001) 014608.

[20] V. Maddalena, *Single-neutron knockout reactions: Application to the spectroscopy of* $^{16,17,19}C$, Phyis. Rev. **C 63** 024613.

[21] A. Bonaccorso and D.M. Brink, *Nucleon Transfer to Continuum States*, Phys. Rev. **C 38** (1988) 1776.

[22] D. Cortina-Gil et al. , *Shell Structure of the Near-Dripline Nucleus* ^{23}O, Phys. Rev. Lett. **93** (2004) 062501.

[23] H. Geissel et al. , *A versatile magnetic system for relativistic heavy ions*, Nucl. Inst. Meth. **B 70** (1992) 286.

[24] D Bianchi et al. , *SPEG: An energy loss spectrometer for GANIL* , Nucl. Instr. Meth. **A 276** (1989) 509.

[25] D.J. Morrissey et al., *A New High-resolution Separator for High Intensity Secondary Beams*, Nucl. Instrum. Meth. **B 126** (1997) 316.

[26] W. Mittig , *Spectromètres magnetiques et electriques comme detecteurs de haute resolution et comme filtres selectifs*, Ecole Joliot-Curie (1994).

[27] Th. Baumann , *Longitudinal momentum distributions of* ^{8}B *and* ^{19}C*: signatures for one-proton and one-neutron halos*, PhD Dissertation, University of Giessen (1999).

[28] Th. Baumann et al., *Longitudinal momentum distributions of* $^{16,18}C$ *fragments after one-neutron removal from* $^{17,19}C$, Phys. Lett. **B 439** (1998) 256.

[29] J. Eberth et al., *MINIBALL A Ge detector array for radioactive ion beam facilities*, Prog. in Part. and Nucl. Pys. **46** (2001) 389.

[30] M. Honma et al., *Effective interaction for pf-shell nuclei*, Phys. Rev. **C 65** (2002) 061301.

[31] P. Maierbeck et al., *Probing the single particle structure around* ^{54}Ca *with knockout reacyions*, Procc. of Finustar conference 2007

[32] N.A. Orr et al., *Momentum Distributions of* ^{9}Li *Fragment Following the Breakup of* ^{11}Li, Phys. Rev. Lett. **69** (1992) 2050.

[33] A. Gade et al., *One-neutron knockout in the vicinity of N=32 sub-shell closure:* $^{9}Be(^{57}Cr,^{56}Cr+\gamma)X$, Phys. Rev. **C 74** (2006) 047302.

[34] C. Rodriguez, *PhD Thesis Universidad de Santiago de Compostela*, on progress.

[35] E. Sauvan et al., *One-Neutron Removal Reactions on Neutron-Rich psd-Shell Nuclei*, Phys. Lett **B 491** (2000) 1.
E. Sauvan et al., *One-neutron removal reactions on light neutron-rich nuclei* , Phys. Rev **C 69** (2004) 044603.

[36] B. Jonson, *Light dripline nuclei*, Phys. Rep. 289 (2004) 1

[37] T. Aumann et al., *One-Neutron Knockout from Individual Single-Particle States of* ^{11}Be, Phys. Rev. Lett **84** (2000) 35.

[38] D. J. Millener et al., *Strong E1 Transitions in* ^{9}Be, ^{11}Be, *and* ^{13}C, Phys. Rev. **C 28** (1983) 497.

[39] J. H. Kelley et al., *Parallel Momentum Distributions as a Probe of Halo Wave Functions*, Phys. Rev. Lett. **74** (1995) 30.

[40] J. Hüfner and M. C. Nemes, *Relativistic heavy ions measure the momentum distribution on the nuclear surface*, Phys. Rev. **C 23** (1981) 2538.

[41] A. Navin et al., *Spectroscopy of Radioactive Beams from Single-Nucleon Knockout Reactions: Application to the sd shell nuclei* ^{25}Al *and* $^{26,27,28}P$, Phys. Rev. Lett. **81** (1998) 5089.

[42] H. Sagawa, B. A. Brown, and H. Esbensen,*Parity inversion in the N=7 isotones and the pairing blocking effect*, Phys. Lett. **B 309** (1993) 1.

[43] F. M. Nunes, I. J. Thompson, and R. C. Johnson, *Core Excitation in One Neutron Halo Systems*, Nucl. Phys. **A 596** (1996) 171.

[44] T. Suzuki, T. Otsuka, and A. Muta, *Magnetic Moment of* ^{11}Be, Phys. Lett. **B 364** (1995) 69.

[45] D. L. Auton, *Direct Reactions on* ^{10}Be, Nucl. Phys. **A 157** (1970) 305.

[46] B. Zwieglinski, W. Benenson, and R. G. H. Robertson, *Study of the* $^{10}Be(d, p)^{11}Be$ *Reaction at 25 MeV*, Nucl. Phys. **A 315** (1979) 124.

[47] N. K. Timofeyuk and R. C. Johnson, *Deuteron Stripping and Pick-Up on Halo Nuclei*, Phys. Rev. **C 59** (1999) 1545.

[48] R. Anne et al., *Exclusive and Restricted-Inclusive Reactions Involving the* ^{11}Be *One-Neutron Halo*, Nucl. Phys. **A 575**(1994) 125.

[49] T. Nakamura et al., *Exclusive and Restricted-Inclusive Reactions Involving the* ^{11}Be *One-Neutron Halo* , Phys. Lett. **B 331**(1994) 296.

[50] E. K. Warburton and B. A. Brown, *Effective Interactions for the 0p1s0d Nuclear Shell-Model Space*,Phys. Rev. **C 46** (1992) 923.

[51] W. Schwab et al., *Obsevation of a proton-halo in* ^{8}B, Zeit. Phys. **A 350** (1995) 283.

[52] M.H. Smedberg et al., *New results on the halo structure of* ^{8}B, Phys. Lett. **B 452** (1999) 1

[53] D. Cortina-Gil et al., *One-Nucleon Removal Cross-Sections for* $^{17,19}C$ *and* $^{8,10}B$, Eur. Phys. J. **A 10** (2001) 49

[54] J.N. Bahcall et al., *How Uncertain are Solar Neutrino Predictions ?* , Phys. Lett. **B 433** (1998) 1

[55] Q. R. Ahmad et al., *Measurement of the Rate of* $\nu_e + d \rightarrow p + p + e$- *Interactions Produced by* ^{8}B *Solar Neutrinos at the Sudbury Neutrino Observatory* , Phys. Rev. Lett. **87** (2001) 071301

[56] D. Cortina-Gil et al., *Experimental Evidence for the 8B Ground State Configuration*, Phys.Lett. **B 529** (2002) 36

[57] M. Staniou et al., *N = 14 and 16 shell gaps in neutron-rich oxygen isotopes*, Phys. Rev. **C 69** (2004) 0234312 .

[58] R. Kanungo et al., *Experimental Evidence of Core Modification in the Near Drip-Line Nucleus* ^{23}O, Phys. Rev. Lett. **88** (2002) 142502.

[59] J.Tostevin, *Core Excitation in Halo Nucleus Break-Up*, Jour. Phys. **G 25** (1999) 735.

[60] B.A. Brown, P.G. Hansen and J.A. Tostevin., *Comment on Experimental Evidence of Core Modification in the Near Drip-Line Nucleus* ^{23}O, Phys. Rev. Lett **90** (2003) 159201

[61] S. Gales, Ch .Stoyanov, A.I. Vdovin, *Damping of High-Lying Single-Particle Modes in Heavy Nuclei*, Phys. Rep. **166** (1988) 125

[62] J.F. Tostevin,, Invited plenary talk at INPC07, June (2007) Tokyo. Proceedings to be published in Nucl. Phys. A

[63] W.H. Dickhoff and C. Barbieri, *Self-consistent Green's function method for nuclei and nuclear matter*, Prog. in Part. and Nucl. Phys. **52** (2004) 377

[64] A. Gade et al., *Reduced Occupancy of the Deeply Bound 0d5=2 Neutron State in* ^{32}Ar, Phys. Rev. Lett. **93** (2004) 042501

[65] G. Baur, C.A. Bertulani, *Coincidence Cross Sections for the Dissociation of Light Ions in High-Energy Collisions* , Nucl. Phys. **A 480** (1988) 615

[66] G. Baur, C.A. Bertulani, H. Rebel, *Coulomb Dissociation as a Source of Information on Radiative Capture Processes of Astrophysical Interest* , Nucl. Phys. **A 458** (1986) 188

[67] C.A. Bertulani,G. Baur, *Electromagnetic processes in heavy ion collisions*, Phys. Rep. **163** (1988) 299

[68] R. Palit et al., *Exclusive measurement of breakup reactions with the one-neutron halo nucleus* ^{11}Be, Phys. Rev. **C 68** (2003) 034318

[69] N. Fukuda et al., *Coulomb and nuclear breakup of a halo nucleus* ^{11}Be, Phys. Rev. **C 70** (2004) 054606

[70] U. Datta-Pramanik et al., *Coulomb breakup of the neutron-rich isotopes* ^{15}C *and* ^{17}C, Phys. Lett. **B 551** (2003) 63

[71] T. Nakamura et al., , *Coulomb Dissociation of* ^{19}C *and Its Halo Structure*, Phys. Rev. Lett. **83** (1999) 1112

[72] C. Nociforo et al., *Coulomb breakup of* ^{23}O, Phys. Lett. **B 605** (2005) 79

[73] J.R. Terry et al., *Direct evidence for the onset of intruder configurations in neutron-rich Ne isotopes* , Nucl. Phys. **A 640** (2006) 86

[74] A. Obertelli et al., *$N = 16$ subshell closure from stability to the neutron drip line*, Phys. Rev. **C 71** (2005) 024304.

[75] J. Tostevin, G. Podolyak, B.A. Brown and P.G. Hansen, *Correlated two-nucleon stripping reactions*, Phys. Rev **C 70** (2004) 064602

[76] J.A. Tostevin and B.A. Brown, *Diffraction dissociation contributions to two-nucleon knockout reactions and the suppression of shell-model strength*, Phys. Rev. **C 74** (2006) 064604

[77] K. Yoneda et al., *Two-neutron knockout from neutron-deficient* ^{34}Ar, ^{30}S, *and* ^{26}Si , Phys. Rev. **C 74** (2006) 021303

[78] A. Gade et al., *Cross-shell excitation in two-proton knockout: Structure of* ^{52}Ca, Phys.Rev. **C 74** (2006) 021302

[79] A. Gade et al., *Spectroscopy of* ^{36}Mg*: Interplay of Normal and Intruder Configurations at the Neutron-Rich Boundary of the Island of Inversion*, Phys. Rev. Lett. **99** (2007) 072502